

Spiral and Mixed Plaquette-Dimer Phases in the $S = 1$ and $3/2$ Shastry-Sutherland Heisenberg Model

Han-Qing Wu^{1,*}, Muwei Wu^{1,2}, and Shou-Shu Gong³

¹*Institute of Neutron Science and Technology, Guangdong Provincial Key Laboratory of Magnetolectric Physics and Devices, School of Physics, Sun Yat-sen University, Guangzhou, 510275, China*

²*Department of Physics, The Chinese University of Hong Kong, Shatin, New Territories, Hong Kong, China*

³*School of Physical Sciences, Great Bay University, Dongguan 523000, China*

Great Bay Institute for Advanced Study, Dongguan 523000, China

(Dated: May 26, 2026)

We investigate the ground-state phase diagram of the $S = 1$ and $S = 3/2$ Heisenberg model on the two-dimensional Shastry-Sutherland lattice (SSL) using density matrix renormalization group (DMRG) and cluster mean-field theory (CMFT). Between the dimer phase and Néel antiferromagnetic phases, we identify two intermediate phases: a mixed plaquette-dimer (MPD) phase and a spiral phase. These phases are characterized via bond energies and spin-spin correlation functions; phase boundaries are located from the ground-state energy derivative and entanglement entropy. The MPD phase exhibits strong intradimer correlations and weak tetramerization on the empty plaquettes, and its transitions to the dimer and spiral phases are first order. Combining our results with the known boundaries for $S = 1/2$ and the classical limit $S \rightarrow \infty$, we construct a global S - g phase diagram. This diagram reveals the progressive suppression of quantum effects with increasing S and offers a theoretical framework for larger- S SSL materials.

Introduction. The Shastry-Sutherland lattice (SSL), formed by adding alternating diagonal couplings J' to a square lattice with nearest-neighbor coupling J , is a paradigmatic model of geometric frustration [1]. For the $S = 1/2$ Heisenberg antiferromagnet with $g = J/J'$, the phase diagram contains dimer, empty-plaquette (EP), and Néel antiferromagnetic (NAF) phases [2–20]. Numerical studies also point to a possible quantum spin liquid (QSL) between the EP and NAF phases [10–12, 18, 19]. Even without a stable QSL, the EP-NAF transition remains intensely debated, with proposals ranging from a deconfined quantum critical point to a weakly first-order transition [6, 8, 14, 15, 17, 21–23]. In the classical limit $S \rightarrow \infty$, quantum order vanishes and a spiral phase emerges for $0 < g < 1$, transitioning into the NAF phase precisely at $g_c=1$ [24, 25]. Clarifying how this intricate phase diagram evolves from the extreme quantum $S = 1/2$ regime to the classical limit is an open challenge.

On the experimental side, $\text{SrCu}_2(\text{BO}_3)_2$ is the first material realization of the SSL, hosting $S = 1/2$ moments on Cu^{2+} ions [26–39]. It enables the exploration of quantum criticality via external magnetic fields and pressure [17, 37, 38, 40]. More recently, new SSL compounds such as $\text{RE}_2\text{Be}_2\text{GeO}_7$ ($\text{RE} = \text{Pr}, \text{Nd}, \text{Gd-Yb}$), ErB_4 and $\text{Eu}_2\text{MgSi}_2\text{O}_7$ have been synthesized [41–49]. Owing to strong spin-orbit coupling, the rare-earth ions can form effective $S = 1/2$ doublets, carry larger spins S , or exhibit XYZ anisotropy [50]. These developments call for a systematic understanding of larger- S SSL physics. As a fundamental step, we investigate the isotropic Heisenberg model with larger S on the SSL.

In this Letter, we determine the ground-state phase diagram of the isotropic Heisenberg model on the SSL for $S = 1$ and $S = 3/2$, using density matrix renormalization group (DMRG) [51, 52] and cluster mean-field theory (CMFT) with DMRG as a solver [20]. We identify two intermediate phases between the dimer and NAF: a mixed plaquette-dimer (MPD) phase and a spiral phase, characterized via bond energies and spin-spin correlations. The spiral phase signals the evolution from the extreme quantum limit ($S = 1/2$) toward the classical regime ($S \rightarrow \infty$): its stability region expands continuously with S , eventually covering the entire interval $0 < g < 1$ in the classical limit. The MPD phase exhibits strong intradimer correlations and weak tetramerization on the empty plaquette; as S increases, its stability window shrinks and shifts to smaller g . These results bridge the gap between the well-studied $S = 1/2$ and classical limits, providing a theoretical framework for larger- S SSL materials.

Model and Method. We consider the SSL depicted as a square lattice with alternating diagonal bonds [Fig. 1(a)]. The Heisenberg Hamiltonian is

$$H = J \sum_{\langle i,j \rangle} \mathbf{S}_i \cdot \mathbf{S}_j + J' \sum_{\langle\langle i,j \rangle\rangle'} \mathbf{S}_i \cdot \mathbf{S}_j,$$

where J and J' denote the nearest-neighbor (inter-dimer) and diagonal (intra-dimer) couplings, depicted as solid and dashed lines in Fig. 1(a). We set $J' = 1$ as energy unit and define the coupling ratio $g = J/J'$. Ground states are determined using DMRG, mostly on cylinders of width $L_y = 4, 6$ and length $L_x = 24$, which can accommodate the incommensurate spiral correlations. Up to 8000 $\text{SU}(2)$ -symmetric states are retained, giving a truncation error below 5×10^{-6} . To characterize the spiral phase further, we employ cluster mean-field theory (CMFT) with DMRG as impurity solver, using the ITen-

* wuhanq3@mail.sysu.edu.cn

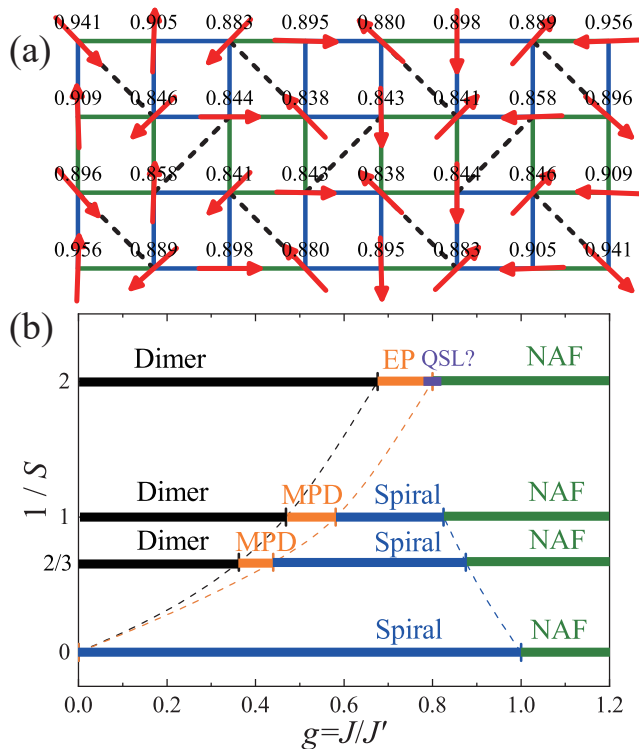


FIG. 1. (a) Cylinder geometry with $L_y = 4, L_x = 8$. Solid (dashed) lines: J (J') bonds. Empty plaquettes (without J') are colored to indicate two distinct bond-energy patterns (olive and blue). Red arrows show the normalized spin moments $\langle S_i \rangle / S$ obtained by CMFT for $S = 3/2$ at $g = 1/\sqrt{2}$, with the magnitudes labeled. (b) Phase diagram as a function of $g = J/J'$ for $S = 1/2, 1, 3/2$, and the classical limit. Dashed lines are guides to the eye. The shaded region marks a possible quantum spin liquid (QSL) phase for $S = 1/2$ (see text).

sor library [20, 53]. CMFT calculations use $L_x = 8$ or 16 , $L_y = 4$ clusters with open boundaries; intercluster interactions are treated at the mean-field level. The DMRG truncation error in these CMFT runs is kept below 10^{-6} .

$S = 1$ numerical results. Figure 2 summarizes the DMRG results for $S = 1$. The second derivative of the ground-state energy per site, $-\partial^2 e_0 / \partial g^2$, shown in Fig. 2(a), exhibits two sharp features at $g_{c1} \approx 0.47$ and $g_{c2} \approx 0.58$. These features, whose apparent divergence depends on the density of sampled g points, signal first-order phase transitions. The bipartite entanglement entropy $S_e = -\text{tr} \rho_l \ln \rho_l$ in Fig. 2(b) independently confirms this picture: it displays clear jumps at both g_{c1} and g_{c2} , making these two transitions more prominent. A broad peak in $-\partial^2 e_0 / \partial g^2$ around $g \approx 0.675$ is likely a finite-size precursor of the transition at g_{c2} ; its position shifts toward g_{c2} as the system size grows, closely resembling the behavior reported for the $S = 1$ orthogonal dimer chain model [54]. Thus, at least two quantum phase transitions occur within $g \in [0, 1]$.

As in the $S = 1/2$ case, the small- g ground state is a dimer phase. At $g = 0$, the exact ground state wave function is a product of dimer singlets $\prod_n \frac{1}{\sqrt{3}} (|1, -1\rangle_n - |0, 0\rangle_n + |-1, 1\rangle_n)$, where n indexes diagonal dimers. For large g , the system enters the NAF phase. A natural expectation is that just above g_{c1} an EP phase appears. To examine this intermediate regime, we focus on $g = 0.5$ and show in Fig. 2(e) the spin structure factor, together with the nearest- and next-nearest-neighbor bond energies on a $L_x = 24, L_y = 6$ cylinder (Fig. 2(i)) and on a fully open cluster (Fig. 2(j)). The spin structure factor reveals only short-range spin correlation for $g \in [g_{c1}, g_{c2}]$. Unlike the $S = 1/2$ EP phase, the bond energies display strong intradimer correlations accompanied by weak tetramerization on the empty plaquettes [Fig. 2(j)]. These features identify a mixed plaquette-dimer (MPD) phase. Like the EP phase, the MPD phase has a two-fold degenerate ground state, corresponding to spin tetramers localized on one of the two empty plaquette sublattices [see olive and blue plaquettes in Fig. 1(a)]. In cylinder geometry, the superposition of the two degenerate states masks the weak tetramerization signal [Fig. 2(i)]. Applying open boundary conditions lifts this degeneracy and makes the spin-tetramer character clearly visible in finite systems, as shown in Fig. 2(j). The tendency toward tetramerization is also reflected in the real-space spin correlations along the x -direction at $g = 0.5$ [Fig. 2(c)], which exhibit a sawtooth-like exponential decay.

For $g > g_{c2}$, the DMRG data show that the system does not immediately enter the NAF phase. Instead, it passes through a spiral phase characterized by a wave vector $\mathbf{q} = (q_x, \pi)$ that varies with g , before eventually locking into the $\mathbf{q} = (\pi, \pi)$ NAF order. A similar phase was recently reported for the $S = 1/2$ XXZ model on the SSL [20]. Figures 2(e)-2(h) display the static spin structure factor $S(\mathbf{q}) = \frac{1}{N_s} \sum_{ij} e^{i\mathbf{q}(\mathbf{r}_j - \mathbf{r}_i)} \langle S_i S_j \rangle / [S(S+1)]$ at $g = 0.5, 0.6, 0.75$, and 0.9 , respectively. A strong magnetic Bragg peak at (q_x, π) is observed. For g below a third critical value g_{c3} , q_x is unlocked from π and shifts continuously with g , a hallmark of incommensurate spiral order. We track this evolution by plotting q_x/π versus g in Fig. 2(d). The wave vector reaches π at $g_{c3} \approx 0.825$, which lies below the $g_{c3} = 1$ in the $S \rightarrow \infty$ classical limit. Further support of g_{c3} comes from the real-space spin correlations shown in Fig. 2(c): in the spiral regime they decay as a power law with spatial oscillations, whereas for $g > g_{c3}$ they revert to a monotonic power-law decay characteristic of the NAF phase. Hence, the $S = 1$ Heisenberg model on the SSL hosts two intermediate phases between dimer and NAF orders: an MPD phase and a spiral phase. Because of finite-size constraints in resolving incommensurate wave vectors, the spiral transition leaves no clear signature in the energy derivative [Fig. 2(a)]. In contrast, the entropy S_e in Fig. 2(b) reveals it through a sharp drop followed by a plateau as g increases.

To characterize the spiral order more directly, we apply CMFT with DMRG solver at the coupling ratio

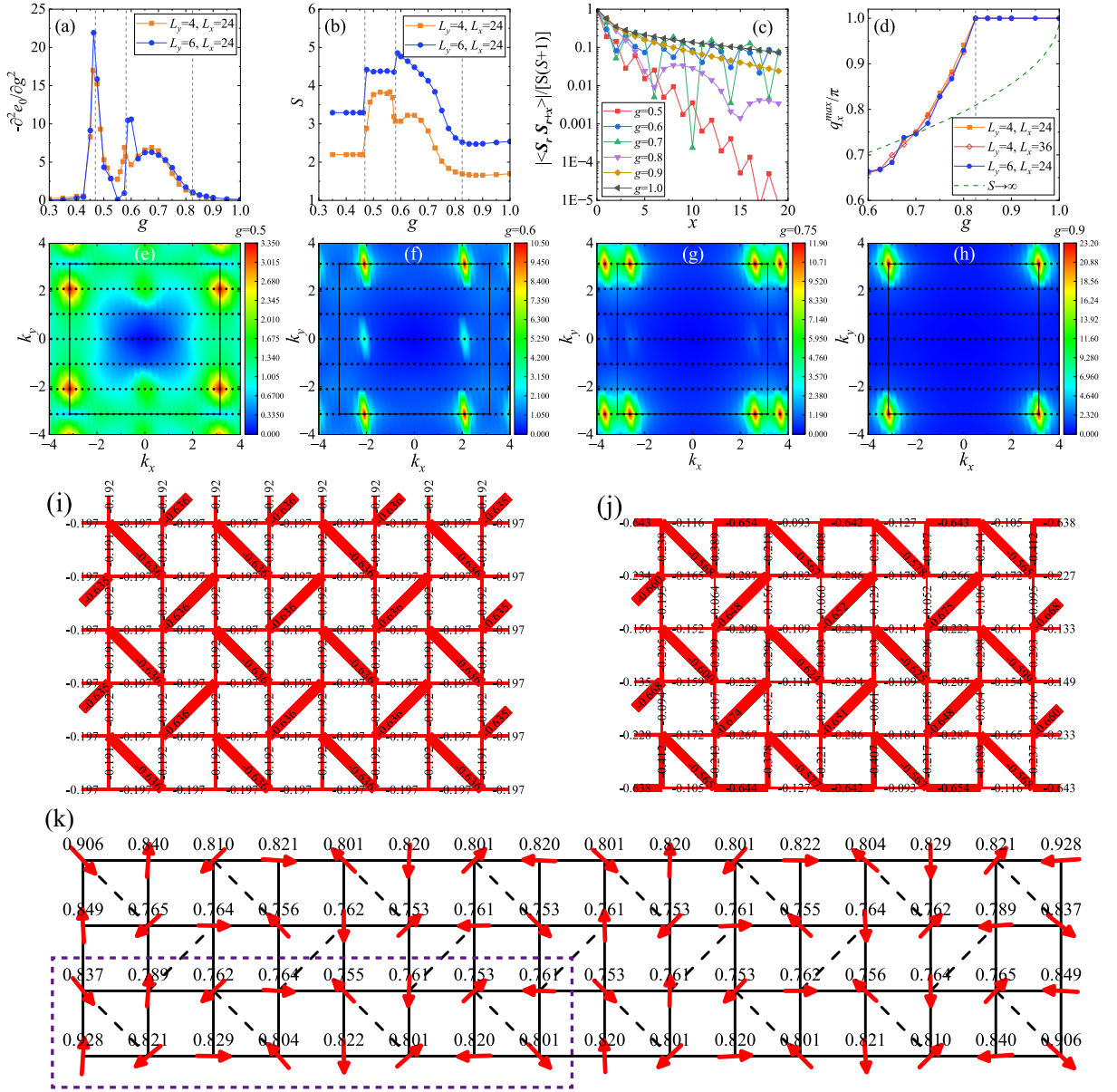


FIG. 2. Numerical results for $S = 1$. Vertical dashed lines in (a), (b), and (d) mark the phase transition points. (a) Second derivative of the ground-state energy per site as a function of the coupling ratio g . Orange and blue curves correspond to $L_y = 4$ and $L_y = 6$ cylinders, respectively. (b) Bipartite entanglement entropy S_e versus g . (c) Real-space spin-spin correlation $|\langle \mathbf{S}_r \mathbf{S}_{r+x} \rangle| / [S(S+1)]$ along the x direction for selected g values. (d) Shift of the magnetic Bragg peak toward $M = (\pi, \pi)$ for $g \in [0.6, 1.0]$. Orange and blue curves correspond to different cylinder widths, and the olive dashed line represents the classical limit $S \rightarrow \infty$. (e-h) Spin structure factors $S(\mathbf{q})$ at $g = 0.5, 0.6, 0.75$, and 0.9 , respectively. (i) Middle part of nearest-neighbor and next-nearest-neighbor bond energies at $g = 0.5$ on the $L_y = 6, L_x = 24$ cylinder. (j) Same as (i), but with open boundary conditions in all directions, making the EP bond pattern evident. (k) Normalized spin moments $\langle \mathbf{S}_i \rangle / [S(S+1)]$ at $g = 1/\sqrt{2}$ from CMFT on an $L_y=4, L_x=16$ cluster. The purple dashed box indicates the magnetic unit cell.

$g = 1/\sqrt{2}$. This value is chosen because the $q_x - g$ curves for $S = 1$ and the classical $S = \infty$ limit intersect there, yielding a spiral with a period-8 oscillation along x for different spin magnitudes [24, 25]. Figure 2(k) presents the resulting spin texture: the directions of the magnetic moments display a clear 8×2 periodicity, while the magnitudes show some deviations from perfect periodicity

due to boundary effects.

We note that A. Koga *et al.* previously studied the $S = 1$ Heisenberg model on the SSL using exact diagonalization on a 4×4 torus [55]. Owing to the limited system size, the phase boundaries were not accurately determined, and the spiral phase, which requires larger systems, was not identified.

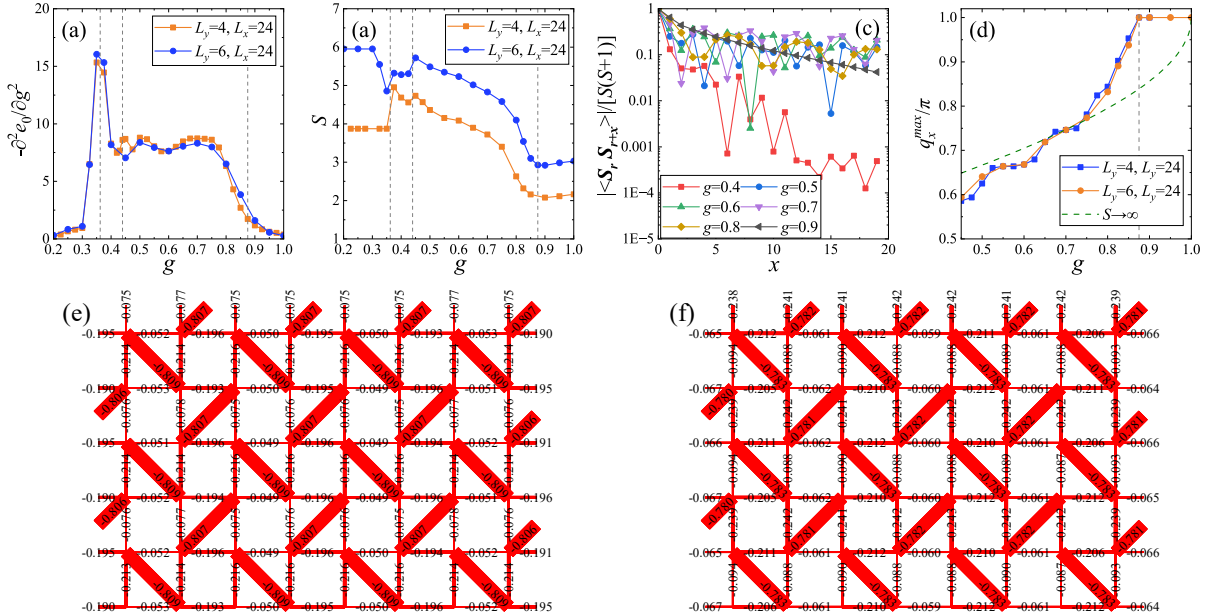


FIG. 3. DMRG results for $S = 3/2$. (a) Second derivative of the ground-state energy per site as a function of the coupling ratio g . Orange and blue curves correspond to $L_y = 4$ and $L_y = 6$ cylinders, respectively. (b) Bipartite entanglement entropy S_e versus g . (c) Real-space spin-spin correlation $|\langle \mathbf{S}_r \cdot \mathbf{S}_{r+x} \rangle|/[S(S+1)]$ along the x direction for selected values of g . (d) Shift of the magnetic Bragg peak toward $M = (\pi, \pi)$ for $g \in [0.45, 1.0]$. Orange and blue curves correspond to different cylinder widths, and the olive dashed line represents the classical limit $S \rightarrow \infty$. (e), (f) Middle part of bond energies at $g = 0.375$ (e) and $g = 0.4$ (f) on an $L_y = 6, L_x = 24$ cylinder. Although both coupling ratios lie within the MPD phase, the two panels reflect the two degenerate tetramerization patterns.

$S = 3/2$ numerical results. Similar to the $S = 1$ case, the $S = 3/2$ Heisenberg model on the SSL exhibits two intermediate phases between the dimer and NAF states: an MPD phase and a spiral phase. The phase transitions are signaled by the second derivative of the energy and by the discontinuous jumps in the entanglement entropy at $g_{c1} \approx 0.36$ and $g_{c2} \approx 0.44$, as shown in Fig. 3(a) and 3(b). Compared to $S = 1$, an additional broad peak emerges in the second derivative of the energy near g_{c3} . The spiral order and the precise value $g_{c3} \approx 0.875$ are identified from the real-space and reciprocal-space spin correlations in Figs. 3(c) and 3(d). For $g_{c2} < g < g_{c3}$, the magnetic Bragg peak (q_x, π) shifts continuously to (π, π) without any intervening phase transition. To examine the MPD phase, we present bond energies at $g = 0.375$ and 0.4 on a $L_x = 24, L_y = 6$ cylinder in Fig. 3(e) and 3(f). Compared to $S = 1$, the spin-tetramerized patterns on the two types of empty plaquettes are more pronounced, even on cylinder geometries, reflecting the two degenerate ground states. We further characterize the spiral order at $g = 1/\sqrt{2}$ via CMFT on an $L_x = 8, L_y = 4$ cluster; the corresponding normalized spin moments $\langle \mathbf{S}_i \rangle / S$ are displayed in Fig. 1(a). These values are closer to unity than those obtained for $S = 1$.

Phase diagram of different S . Combining the phase boundaries determined here for $S = 1$ and $S = 3/2$ with the established results for $S = 1/2$ and the classical limit $S \rightarrow \infty$, we construct the global $S - g$ phase diagram in

Fig. 1(b). For $S = 1/2$, we adopt the transition points $g_{c1} = 0.676$ and $g_{c2} = 0.8$ from Ref. [20]. The proposed quantum spin liquid (QSL) regime is indicated in purple (see, e.g., Refs. [10–12, 18, 19] and references therein). For $S \geq 1$, a spiral phase emerges between the MPD and NAF phases. As S increases, the spiral region expands continuously, while the MPD phase shrinks and shifts toward smaller g until it disappears; the dimer phase likewise diminishes and vanishes in the classical limit. In the $S \rightarrow \infty$ limit, the phase diagram reduces to the classical case, with only the spiral and NAF phases. These results show that even for larger spins, quantum fluctuations combined with geometric frustration can stabilize exotic phases such as the MPD phase, which have no classical counterpart.

Summary and discussion. Using DMRG and CMFT, we have investigated the ground-state phase diagram of the Heisenberg model on the Shastry-Sutherland lattice for $S = 1$ and $3/2$. We identify two intermediate phases between the dimer and NAF phases: a mixed plaquette-dimer (MPD) phase, characterized by strong intradimer correlations and weak tetramerization on the empty plaquettes, and a spiral phase with an incommensurate wave vector (q_x, π) that shifts continuously to (π, π) with increasing g . Combining our results with the known phase boundaries for $S = 1/2$ and the classical limit ($S \rightarrow \infty$), we construct a unified $S - g$ phase diagram spanning from the quantum to classical regimes.

Our results demonstrate that quantum fluctuations and geometric frustration can stabilize nonmagnetic phases, such as the MPD state, even for $S = 3/2$. The spiral phase for $S \geq 1$ bridges the quantum-disordered ground state at $S = 1/2$ and the classical spiral order. Given the recent synthesis of rare-earth-based Shastry-Sutherland materials with effective larger spins, this phase diagram provides a theoretical framework for interpreting experiments and predicting magnetic ground states in these compounds.

ACKNOWLEDGMENTS

H.Q.W. and M.W. are supported by the National Natural Science Foundation of China (Grant No. 12474248), Guangdong Basic and Applied Basic Research Foundation (Grant No. 2023B1515120013), Guangdong Provincial Key Laboratory of Magnetoelectric Physics and Devices (No. 2022B1212010008) and Guangdong Fundamental Research Center for Magnetoelectric Physics (Grant No. 2024B0303390001). S. S. G. was supported by the National Natural Science Foundation of China (No. 12274014 and No. 12534009), the Guangdong Provincial Quantum Science Strategic Initiative (Grant No. GDZX2501006), the Special Project in Key Areas for Universities in Guangdong Province (No. 2023ZDZX3054), and the Dongguan Key Laboratory of Artificial Intelligence Design for Advanced Materials.

-
- [1] B. Sriram Shastry and B. Sutherland, Exact ground state of a quantum mechanical antiferromagnet, *Physica B+C* **108**, 1069 (1981).
- [2] A. Koga and N. Kawakami, Quantum Phase Transitions in the Shastry-Sutherland Model for $\text{SrCu}_2(\text{BO}_3)_2$, *Phys. Rev. Lett.* **84**, 4461 (2000).
- [3] C. H. Chung, J. B. Marston, and S. Sachdev, Quantum phases of the Shastry-Sutherland antiferromagnet: Application to $\text{SrCu}_2(\text{BO}_3)_2$, *Phys. Rev. B* **64**, 134407 (2001).
- [4] A. Läuchli, S. Wessel, and M. Sigrist, Phase diagram of the quadrumerized Shastry-Sutherland model, *Phys. Rev. B* **66**, 014401 (2002).
- [5] J. Lou, T. Suzuki, K. Harada, and N. Kawashima, Study of the shastry sutherland model using multi-scale entanglement renormalization ansatz (2012), [arXiv:1212.1999 \[cond-mat.str-el\]](https://arxiv.org/abs/1212.1999).
- [6] P. Corboz and F. Mila, Tensor network study of the shastry-sutherland model in zero magnetic field, *Phys. Rev. B* **87**, 115144 (2013).
- [7] Z. Zhang and P. Sengupta, Generalized plaquette state in the anisotropic shastry-sutherland model, *Phys. Rev. B* **92**, 094440 (2015).
- [8] J. Y. Lee, Y.-Z. You, S. Sachdev, and A. Vishwanath, Signatures of a Deconfined Phase Transition on the Shastry-Sutherland Lattice: Applications to Quantum Critical $\text{SrCu}_2(\text{BO}_3)_2$, *Phys. Rev. X* **9**, 041037 (2019).
- [9] C. Boos, S. P. G. Crone, I. A. Niesen, P. Corboz, K. P. Schmidt, and F. Mila, Competition between intermediate plaquette phases in $\text{SrCu}_2(\text{BO}_3)_2$ under pressure, *Phys. Rev. B* **100**, 140413 (2019).
- [10] J. Yang, A. W. Sandvik, and L. Wang, Quantum criticality and spin liquid phase in the shastry-sutherland model, *Phys. Rev. B* **105**, L060409 (2022).
- [11] A. Keleş and E. Zhao, Rise and fall of plaquette order in the shastry-sutherland magnet revealed by pseudo-fermion functional renormalization group, *Phys. Rev. B* **105**, L041115 (2022).
- [12] L. Wang, Y. Zhang, and A. W. Sandvik, Quantum spin liquid phase in the shastry-sutherland model detected by an improved level spectroscopic method, *Chin. Phys. Lett.* **39**, 077502 (2022).
- [13] J. Wang, H. Li, N. Xi, Y. Gao, Q.-B. Yan, W. Li, and G. Su, Plaquette singlet transition, magnetic barocaloric effect, and spin supersolidity in the shastry-sutherland model, *Phys. Rev. Lett.* **131**, 116702 (2023).
- [14] N. Xi, H. Chen, Z. Y. Xie, and R. Yu, Plaquette valence bond solid to antiferromagnet transition and deconfined quantum critical point of the shastry-sutherland model, *Phys. Rev. B* **107**, L220408 (2023).
- [15] W.-Y. Liu, X.-T. Zhang, Z. Wang, S.-S. Gong, W.-Q. Chen, and Z.-C. Gu, Quantum Criticality with Emergent Symmetry in the Extended Shastry-Sutherland Model, *Phys. Rev. Lett.* **133**, 026502 (2024).
- [16] G. Duan, R. Yu, and C. Liu, Theory of magnetism for rare-earth magnets on the shastry-sutherland lattice with non-kramers ions, *Phys. Rev. B* **110**, 214410 (2024).
- [17] H. Chen, G. Duan, C. Liu, Y. Cui, W. Yu, Z. Y. Xie, and R. Yu, Spin excitations of the shastry-sutherland model – altermagnetism and proximate deconfined quantum criticality (2024), [arXiv:2411.00301 \[cond-mat.str-el\]](https://arxiv.org/abs/2411.00301).
- [18] L. L. Viteritti, R. Rende, A. Parola, S. Goldt, and F. Becca, Transformer wave function for two dimensional frustrated magnets: Emergence of a spin-liquid phase in the shastry-sutherland model, *Phys. Rev. B* **111**, 134411 (2025).
- [19] P. Corboz, Y. Zhang, B. Ponsioen, and F. Mila, Quantum spin liquid phase in the shastry-sutherland model revealed by high-precision infinite projected entangled-pair states (2025), [arXiv:2502.14091 \[cond-mat.str-el\]](https://arxiv.org/abs/2502.14091).
- [20] Z. Yuan, M. Wu, D.-X. Yao, and H.-Q. Wu, Spiral phase and phase diagram of the $s=1/2$ xxz model on the shastry-sutherland lattice (2026), [arXiv:2601.22924 \[cond-mat.str-el\]](https://arxiv.org/abs/2601.22924).
- [21] T. Senthil, A. Vishwanath, L. Balents, S. Sachdev, and M. P. A. Fisher, Deconfined quantum critical points, *Science* **303**, 1490 (2004).
- [22] Y. Cui, R. Yu, and W. Yu, Deconfined Quantum Critical Point: A Review of Progress, *Chinese Physics Letters* **42**, 047503 (2025).
- [23] L. Chen and Z.-X. Liu, Deconfined gapless phases and criticalities in shastry-sutherland antiferromagnet

- (2025), [arXiv:2503.20122 \[cond-mat.str-el\]](#).
- [24] R. Darradi, J. Richter, and D. J. J. Farnell, Coupled cluster treatment of the shastry-sutherland antiferromagnet, *Phys. Rev. B* **72**, 104425 (2005).
- [25] M. Moliner, D. C. Cabra, A. Honecker, P. Pujol, and F. Stauffer, Magnetization process in the classical heisenberg model on the shastry-sutherland lattice, *Phys. Rev. B* **79**, 144401 (2009).
- [26] H. Kageyama, K. Yoshimura, R. Stern, N. V. Mushnikov, K. Onizuka, M. Kato, K. Kosuge, C. P. Slichter, T. Goto, and Y. Ueda, Exact Dimer Ground State and Quantized Magnetization Plateaus in the Two-Dimensional Spin System $\text{SrCu}_2(\text{BO}_3)_2$, *Phys. Rev. Lett.* **82**, 3168 (1999).
- [27] S. Miyahara and K. Ueda, Exact Dimer Ground State of the Two Dimensional Heisenberg Spin System $\text{SrCu}_2(\text{BO}_3)_2$, *Phys. Rev. Lett.* **82**, 3701 (1999).
- [28] T. Waki, K. Arai, M. Takigawa, Y. Saiga, Y. Uwatoko, H. Kageyama, and Y. Ueda, A Novel Ordered Phase in $\text{SrCu}_2(\text{BO}_3)_2$ under High Pressure, *Journal of the Physical Society of Japan* **76**, 073710 (2007).
- [29] S. Haravifard, A. Banerjee, J. C. Lang, G. Srajer, D. M. Silevitch, B. D. Gaulin, H. A. Dabkowska, and T. F. Rosenbaum, Continuous and discontinuous quantum phase transitions in a model two-dimensional magnet, *Proceedings of the National Academy of Sciences* **109**, 2286 (2012).
- [30] M. Takigawa, M. Horvatić, T. Waki, S. Krämer, C. Berthier, F. Lévy-Bertrand, I. Sheikin, H. Kageyama, Y. Ueda, and F. Mila, Incomplete Devil's Staircase in the Magnetization Curve of $\text{SrCu}_2(\text{BO}_3)_2$, *Phys. Rev. Lett.* **110**, 067210 (2013).
- [31] M. E. Zayed, C. Rüegg, T. Strässle, U. Stuhr, B. Roessli, M. Ay, J. Mesot, P. Link, E. Pomjakushina, M. Stingaciu, K. Conder, and H. M. Rønnow, Correlated Decay of Triplet Excitations in the Shastry-Sutherland Compound $\text{SrCu}_2(\text{BO}_3)_2$, *Phys. Rev. Lett.* **113**, 067201 (2014).
- [32] S. Haravifard, D. Graf, A. E. Feiguin, C. D. Batista, J. C. Lang, D. M. Silevitch, G. Srajer, B. D. Gaulin, H. A. Dabkowska, and T. F. Rosenbaum, Crystallization of spin superlattices with pressure and field in the layered magnet $\text{SrCu}_2(\text{BO}_3)_2$, *Nature Communications* **7**, 11956 (2016).
- [33] M. E. Zayed, C. Rüegg, J. Larrea J., A. M. Läuchli, C. Panagopoulos, S. S. Saxena, M. Ellerby, D. F. McMorrow, T. Strässle, S. Klotz, G. Hamel, R. A. Sadykov, V. Pomjakushin, M. Boehm, M. Jiménez-Ruiz, A. Schneidewind, E. Pomjakushina, M. Stingaciu, K. Conder, and H. M. Rønnow, 4-spin plaquette singlet state in the Shastry-Sutherland compound $\text{SrCu}_2(\text{BO}_3)_2$, *Nature Physics* **13**, 962 (2017).
- [34] J. Guo, G. Sun, B. Zhao, L. Wang, W. Hong, V. A. Sidorov, N. Ma, Q. Wu, S. Li, Z. Y. Meng, A. W. Sandvik, and L. Sun, Quantum Phases of $\text{SrCu}_2(\text{BO}_3)_2$ from High-Pressure Thermodynamics, *Phys. Rev. Lett.* **124**, 206602 (2020).
- [35] J. L. Jiménez, S. P. G. Crone, E. Fogh, M. E. Zayed, R. Lortz, E. Pomjakushina, K. Conder, A. M. Läuchli, L. Weber, S. Wessel, A. Honecker, B. Normand, C. Rüegg, P. Corboz, H. M. Rønnow, and F. Mila, A quantum magnetic analogue to the critical point of water, *Nature* **592**, 370 (2021).
- [36] Z. Shi, S. Dissanayake, P. Corboz, W. Steinhardt, D. Graf, D. M. Silevitch, H. A. Dabkowska, T. F. Rosenbaum, F. Mila, and S. Haravifard, Discovery of quantum phases in the Shastry-Sutherland compound $\text{SrCu}_2(\text{BO}_3)_2$ under extreme conditions of field and pressure, *Nature Communications* **13**, 2301 (2022).
- [37] Y. Cui, L. Liu, H. Lin, K.-H. Wu, W. Hong, X. Liu, C. Li, Z. Hu, N. Xi, S. Li, R. Yu, A. W. Sandvik, and W. Yu, Proximate deconfined quantum critical point in $\text{SrCu}_2(\text{BO}_3)_2$, *Science* **380**, adc9487 (2023).
- [38] Y. Cui, K. Du, Z. Wu, S. Li, P. Yang, Y. Chen, X. Xu, H. Chen, C. Li, J. Liu, B. Wang, W. Hong, S. Li, Z. Xie, J. Cheng, R. Yu, and W. Yu, Two plaquette-singlet phases in the Shastry-Sutherland compound $\text{SrCu}_2(\text{BO}_3)_2$ (2024), [arXiv:2411.00302 \[cond-mat.str-el\]](#).
- [39] J. Guo, P. Wang, C. Huang, B.-B. Chen, W. Hong, S. Cai, J. Zhao, J. Han, X. Chen, Y. Zhou, S. Li, Q. Wu, Z. Y. Meng, and L. Sun, Deconfined quantum critical point lost in pressurized $\text{SrCu}_2(\text{BO}_3)_2$, *Communications Physics* **8**, 75 (2025).
- [40] J. Guo, P. Wang, C. Huang, C. Zhou, M. Song, X. Chen, T.-T. Wang, W. Hong, S. Cai, J. Zhao, J. Han, Y. Zhou, Q. Wu, S. Li, Z. Y. Meng, and L. Sun, T-linear specific heat in pressurized and magnetized shastry-sutherland mott insulator $\text{srCu}_2(\text{bo}_3)_2$ (2026), [arXiv:2602.18229 \[cond-mat.str-el\]](#).
- [41] M. Ashtar, Y. Bai, L. Xu, Z. Wan, Z. Wei, Y. Liu, M. A. Marwat, and Z. Tian, Structure and Magnetic Properties of Melilite-Type Compounds $\text{RE}_2\text{Be}_2\text{GeO}_7$ ($\text{RE} = \text{Pr}, \text{Nd}, \text{Gd-Yb}$) with Rare-Earth Ions on Shastry-Sutherland Lattice, *Inorganic Chemistry* **60**, 3626 (2021), pMID: 33635649.
- [42] M. Pula, S. Sharma, J. Gautreau, S. K. P., A. Kanigel, M. D. Frontzek, T. N. Dolling, L. Clark, S. Dunsiger, A. Ghara, and G. M. Luke, Candidate for a quantum spin liquid ground state in the Shastry-Sutherland lattice material $\text{Yb}_2\text{Be}_2\text{GeO}_7$, *Phys. Rev. B* **110**, 014412 (2024).
- [43] N. Li, A. Brassington, M. F. Shu, Y. Y. Wang, H. Liang, Q. J. Li, X. Zhao, P. J. Baker, H. Kikuchi, T. Masuda, G. Duan, C. Liu, H. Wang, W. Xie, R. Zhong, J. Ma, R. Yu, H. D. Zhou, and X. F. Sun, Spinons in a new Shastry-Sutherland lattice magnet $\text{Pr}_2\text{Ga}_2\text{BeO}_7$ (2024), [arXiv:2405.13628 \[cond-mat.str-el\]](#).
- [44] A. Liu, J. Zhou, L. Wang, Y. Cao, F. Song, Y. Han, J. Li, W. Tong, Z. Xia, Z. Ouyang, J. Zhao, H. Guo, and Z. Tian, Large magnetocaloric effect in the shastry-sutherland lattice compound $\text{Yb}_2\text{Be}_2\text{GeO}_7$ with spin-disordered ground state, *Phys. Rev. B* **110**, 144445 (2024).
- [45] A. Liu, F. Song, Y. Cao, H. Ge, H. Bu, J. Zhou, Y. Qin, Q. Zeng, J. Li, L. Ling, W. Tong, J. Sheng, M. Yang, L. Wu, H. Guo, and Z. Tian, Distinct magnetic ground states in shastry-sutherland lattice materials: $\text{Pr}_2\text{Be}_2\text{GeO}_7$ versus $\text{Nd}_2\text{Be}_2\text{GeO}_7$, *Phys. Rev. B* **109**, 184413 (2024).
- [46] A. Brassington, Q. Huang, A. A. Aczel, and H. D. Zhou, Synthesis and magnetic properties of the Shastry-Sutherland family $R_2\text{Be}_2\text{SiO}_7$ ($R = \text{Nd}, \text{Sm}, \text{Gd-Yb}$), *Phys. Rev. Mater.* **8**, 014005 (2024).
- [47] M. Pula, S. Sharma, J. Gautreau, S. K. P., A. Kanigel, and G. M. Luke, Ground-states of the Shastry-Sutherland lattice materials $\text{Gd}_2\text{Be}_2\text{GeO}_7$ and $\text{Dy}_2\text{Be}_2\text{GeO}_7$ (2025), [arXiv:2505.04868 \[cond-mat.str-el\]](#).
- [48] S. Flury, W. J. Simeth, D. R. Yahne, M. Islam, I. Plokhikh, D. G. Mazzone, E. D. Bauer, P. F. S.

- Rosa, R. Sibille, O. Zaharko, D. J. Gawryluk, and M. Janoschek, Magnetic phase diagram of erb_4 as explored by neutron scattering, *Phys. Rev. B* **112**, 224441 (2025).
- [49] J. Gong, J. Wang, J. Xiang, Z. Mo, L. Zhang, X. Liu, X. He, L. Tian, Z. Ye, H. Xie, X. Kan, X. Gao, Z. Li, P. Sun, S. Wang, W. Li, B. Shen, and J. Shen, Giant magnetocaloric effect in a high-spin Shastry-Sutherland dipolar magnet (2026), [arXiv:2602.08497 \[cond-mat.mtrl-sci\]](https://arxiv.org/abs/2602.08497).
- [50] C. Liu, G. Duan, and R. Yu, Theory of rare-earth Kramers magnets on a shastry-sutherland lattice: dimer phases in the presence of strong spin-orbit coupling, *npj Quantum Materials* **10**, 109 (2025).
- [51] S. R. White, Density matrix formulation for quantum renormalization groups, *Phys. Rev. Lett.* **69**, 2863 (1992).
- [52] U. Schollwöck, The density-matrix renormalization group, *Rev. Mod. Phys.* **77**, 259 (2005).
- [53] M. Fishman, S. R. White, and E. M. Stoudenmire, The ITensor Software Library for Tensor Network Calculations, *SciPost Phys. Codebases*, 4 (2022).
- [54] K. Ren, M. Wu, S.-S. Gong, D.-X. Yao, and H.-Q. Wu, Haldane phases and phase diagrams of the $s = \frac{3}{2}$ and $s = 1$ bilinear-biquadratic heisenberg model on the orthogonal dimer chain, *Phys. Rev. B* **108**, 245104 (2023).
- [55] A. Koga, N. Kawakami, and M. Sigrist, Quantum Phase Transitions of the $S=1$ Shastry-Sutherland Model, *Journal of the Physical Society of Japan* **72**, 938 (2003).